Collaboration between hepatic and intratumoral prodrug activation in a P450 prodrug-activation gene therapy model for cancer treatment

Jie Ma and David J. Waxman

Division of Cell and Molecular Biology, Department of Biology, Boston University, Boston, Massachusetts

Abstract

Presently, we investigate the mechanisms whereby intratumoral expression of a cyclophosphamide-activating hepatic cytochrome *P*450 gene enhances therapeutic activity when cyclophosphamide is given on an every 6-day (metronomic) schedule. In P450-deficient 9L gliosarcomas grown in severe combined immunodeficient mice, metronomic cyclophosphamide substantially decreased tumor microvessel density and induced a ~70% loss of endothelial cells that began after the second cyclophosphamide treatment. These responses were accompanied by increased expression of the endogenous angiogenesis inhibitor thrombospondin-1 in tumor-associated host cells but by decreased expression in 9L tumor cells. These antiangiogenic responses preceded tumor regression and are likely key to the therapeutic activity of metronomic cyclophosphamide. Unexpectedly, 9L/2B11 tumors, grown from 9L cells infected with retrovirus encoding the cyclophosphamide-activating P450 2B11, exhibited antiangiogenic responses very similar to 9L tumors. This indicates that the tumor endothelial cell population is well exposed to liver-activated cyclophosphamide metabolites and that intratumoral *P*450 confers limited additional anti–endothelial cell bystander activity. In contrast, an increase in apoptosis, which preceded the antiangiogenic response, was substantially enhanced by intratumoral P450 2B11 expression. 9L/2B11 tumor regression was accompanied by an overall loss of tumor cellularity and by substantial enlargement of remaining P450-immunoreactive tumor cells as the number of P450-positive tumor cell decreased and the P450 protein content declined with cyclophosphamide treatment. We conclude that metronomic cyclophosphamide regresses P450-expressing tumors by two independent but complementary mechanisms: increased tumor cell killing via intratumoral P450-catalyzed prodrug activation, coupled with strong antiangiogenic activity, which is primarily associated with hepatic prodrug activation. [Mol Cancer Ther 2007;6(11):2879–90]

Introduction

Cancer chemotherapeutic drugs are often administered at their maximum tolerated doses (MTD) to maximize the killing of malignant cells; however, the effectiveness of this approach is limited by the collateral damage to proliferating cells in the intestinal epithelium, bone marrow, and hair follicles. Strategies to improve tumor cell–specific targeting include the use of antibody-cytotoxin or aptamer-cytotoxin conjugates (1, 2), antibody-directed immunoliposomes (3), and systemic delivery of anticancer prodrugs in combination with tumor-specific expression of prodrug-activating enzymes. This latter approach, termed gene-directed enzyme-prodrug therapy, has been studied with a variety of enzyme-prodrug combinations, including cytochrome *P*450 with the oxazaphosphorine alkylating agent prodrug cyclophosphamide. The development of gene-directed enzyme-prodrug therapy strategies combining P450 enzymes with cyclophosphamide has been facilitated by the extensive clinical experience with cyclophosphamide, the diffusibility of its active 4-hydroxy metabolite, and the associated bystander cytotoxic effect. P450-based gene-directed enzyme-prodrug therapy has been exemplified in preclinical studies using vectors based on retrovirus (4), herpes virus (5), and adenovirus (6) and by using encapsulated cells engineered to express cytochrome *P*450 (7). P450-based gene-directed enzyme-prodrug therapy substantially improves antitumor activity in preclinical studies, and initial clinical trials have been positive (8, 9).

Much progress has been made since angiogenesis was first proposed as a target for cancer therapy (10), with several antiangiogenic agents now in clinical use (11). When administered at a low dose but at frequent intervals (i.e., a metronomic schedule), cyclophosphamide and several other traditional chemotherapeutic drugs show antiangiogenic activity and inhibit tumor growth in xenograft models, whereas the same drug given at a similar total dose but using a MTD regimen is much less effective (12–16). In clinical trials, daily low-dose cyclophosphamide given in combination with other chemotherapeutic drugs provides clinical benefit with minimal toxicity to patients with advanced solid tumors (17, 18). Traditional chemotherapeutics administered on a metronomic schedule may find use as cost-effective alternatives to new and expensive antiangiogenic drugs now in development (19).

Received 4/26/07; revised 7/13/07; accepted 9/18/07.

Grant support: NIH grant CA49248 (D.J. Waxman).

The costs of publication of this article were defrayed in part by the payment of page charges. This article must therefore be hereby marked *advertisement* in accordance with 18 U.S.C. Section 1734 solely to indicate this fact.

Requests for reprints: David J. Waxman, Department of Biology, Boston University, 5 Cummington Street, Boston, MA 02215. Fax: 617-353-7404. E-mail: djw@bu.edu

doi:10.1158/1535-7163.MCT-07-0297

Compared with a MTD regimen, metronomic cyclophosphamide shows substantially enhanced antitumor activity in the rat 9L gliosarcoma model (13, 20); however, the role of tumor cell cytotoxicity versus antiangiogenesis in the observed therapeutic response is unclear. Introduction of a prodrug-activating P450 gene into tumor cells accelerates tumor regression and extends the tumor-free period following metronomic cyclophosphamide treatment (20), but it is not known how P450-catalyzed intratumoral drug activation affects the antiangiogenic response. In particular, it is unclear whether the therapeutic activity of P450-based gene-directed enzyme-prodrug therapy primarily results from an increase in direct tumor cell killing, or whether the localized production of active drug metabolites enhances the antiangiogenic response. To address these issues, we presently investigate the changes in tumor vascularization and apoptosis in a tumor xenograft model expressing P450 2B11, a highly efficient catalyst of cyclophosphamide activation characterized by an atypically low K_m (21). We also study the effect of metronomic cyclophosphamide treatment on the expression of the cyclophosphamide-activating P450 enzyme. Our findings show that P450-based gene-directed enzyme-prodrug therapy enhances antitumor activity primarily by chemosensitizing tumor cells, without changing activity against tumor-associated endothelial cells. Overall antitumor activity is thus optimized when P450 gene delivery is combined with tumor endothelial cell–directed metronomic cyclophosphamide treatment.

Materials and Methods

Chemicals and Antibodies

Cyclophosphamide (C0768), collagenase type IV (C5138), DNase I (D5025), and mouse monoclonal anti–smooth muscle actin-α antibody (A5228) were purchased from Sigma-Aldrich Co. Fetal bovine serum (FBS), DMEM, and TRIzol reagent were purchased from Invitrogen. Paraformaldehyde solution (16%; methanol-free) was purchased from Electron Microscopy Sciences. FITC-conjugated or unconjugated rat monoclonal anti-CD31 antibody (immunoglobulin G2a) and FITC-conjugated rat immunoglobulin G2a were purchased from BD Bioscience. Mouse monoclonal anti–TSP-1 antibody (MS-421; reactive with rat and mouse TSP-1) was purchased from Lab Vision Co. Goat polyclonal anti–TSP-1 antibody (sc-12312; reactive with mouse TSP-1) was purchased from Santa Cruz Biotechnology. Rabbit polyclonal anti–P450 2B11 antibody was a gift from Dr. James Halpert (University of Texas Medical Branch, Galveston, TX). Mouse monoclonal anti–P450 2B6 antibody (A326) was purchased from BD Gentest. Horseradish peroxidase–conjugated donkey anti-rabbit antibody (NA934) was from Amersham Biosciences. Normal horse serum, normal rabbit serum, avidin/biotin blocking kit, biotinylated secondary antibodies (horse anti-mouse antibody BA-2000, rabbit anti-goat antibody BA-5000, and rabbit anti-rat antibody BA-4000), Vectastain Elite ABC Kit, peroxidase substrates (3,3′-diaminobenzidine, 3,3′,5,5′-tetramethylbenzidine, and VIP), VectaMount, and Gill's hematoxylin were from Vector Laboratories. DeadEnd Colorimetric terminal deoxyribonucleotidyl transferase–mediated dUTP nick end labeling (TUNEL) kit and RNase-free DNase (M6101) were from Promega. Alcoholic eosin Y (1%) was purchased from Fisher Scientific. Random hexamers, MuLV reverse transcriptase, RNase inhibitor, and SYBR Green PCR Master Mix were purchased from Applied Biosystems. Dc Protein Assay kit was purchased from Bio-Rad. SuperSignal West Femto Maximum Sensitivity Substrate was purchased from Pierce Biotechnology.

Tumor Cell Lines

9L rat gliosarcoma cells infected with retrovirus encoding P450 reductase in combination with either P450 2B11 or P450 2B6 (9L/2B11 and 9L/2B6 cells, respectively) and 9L tumor cells infected with the empty retroviral vector pBabe (9L/pBabe cells, herein referred to as 9L cells) were described previously (20).

Tumor Growth Delay Experiments

Male Fox Chase ICR severe combined immunodeficient (SCID) mice (Taconic Farms) were housed in the Boston University Laboratory Animal Care Facility in accordance with approved protocols and federal guidelines. Autoclaved cages containing food and water were changed weekly. Mouse body weight was monitored every 3 days. 9L, 9L/2B11, and 9L/2B6 cells used for tumor inoculation were grown in DMEM containing 10% FBS, trypsinized, resuspended in FBS-free DMEM at a concentration of 8×10^6 cells/mL, then kept on ice until injection. Cells, 4×10^6 in a volume of 0.5 mL, were injected s.c. into each flank of a 5-week-old SCID mouse using a 27-gauge needle. Tumor sizes (length L × width W) were measured every 3 days using vernier calipers (Manostat Co.) and volumes (V) calculated as $V = (\pi/6) \times (L \times W)^{3/2}$. Cyclophosphamide treatment was initiated when the average tumor volume reached ~500 mm^3. Fresh cyclophosphamide solution dissolved in PBS (140 mmol/L NaCl, 10 mmol/L Na_2HPO_4, 2.7 mmol/L KCl, 1.8 mmol/L KH_2PO_4) was filtered through a 0.2-μm Acrodisc syringe filter (Pall Co.) and administered to the tumor-bearing mice by i.p. injection at 140 mg cyclophosphamide/kg body weight every 6 days (13).

Tumor Cryosectioning and Immunohistochemistry

Fresh tumor tissues were snap-frozen in dry ice-cold 2-methylbutane and stored at −80°C. Tumor cryosections (6 μm; 3–4 sections per slide) were prepared using a Leica 1800 cryostat and fixed with 1% paraformaldehyde at room temperature for 30 min. Following a PBS wash, the sections were incubated with permeabilization solution containing 1% Triton X-100 (v/v) and 1% sodium citrate (w/v) for 5 min on ice followed by a second PBS wash. Sections were blocked at room temperature for 20 min with PBS containing 2% normal serum from the species in which the secondary antibody was raised, except for normal horse serum, which was used in place of normal donkey serum. The slides were then incubated with primary antibody for 1 h at 37°C followed by a PBS wash. The secondary

antibody was also incubated for 1 h at 37°C followed by another PBS wash. The sections were then incubated with ABC complex for 30 min at room temperature. Peroxidase substrate (3,3′-diaminobenzidine, 3,3′-diaminobenzidine-nickel, 3,3′,5,5′-tetramethylbenzidine, or VIP) was added and color development was terminated by immersing the slides in tap water. After hematoxylin counterstaining, the slides were dehydrated by sequential washing with 95% ethanol, 100% ethanol, and 100% xylene and sealed with VectaMount. The final concentration of each primary antibody was as follows: CD31, 0.3 μg/mL; P450 2B6, 1:2,000 dilution; P450 2B11, 8 μg/mL; smooth muscle actin-α, 5 μg/mL; and TSP-1, 4 μg/mL for antibody MS-421 and 2 μg/mL for antibody sc-12312. Secondary antibodies were diluted to 7.5 μg/mL (biotinylated antigoat, anti-mouse, and antirat antibodies) or 1:500 (horseradish peroxidase–conjugated antirabbit antibody). Because of the different sensitivities of each primary antibody and peroxidase substrate, CD31/3,3′-diaminobenzidine staining was always carried out first when samples were double immunostained, followed by staining with anti–TSP-1 (sc-12312)/3,3′,5,5′-tetramethylbenzidine or anti–smooth muscle actin-α/3,3′,5,5′-tetramethylbenzidine. Avidin/biotin blocking kit was used for double immunostaining per manufacturer's protocol.

Tumor Microvessel Density

CD31-stained tumor sections were examined using an Olympus BX50 bright-field light microscope. A representative section was identified for each tumor and the number of blood vessels was counted in five random fields per section at a magnification of ×400. Microvessel density was presented as mean ± SE for four individual tumors per treatment group at each time point.

Preparation of Single-Cell Suspension from Fresh Tumor Tissue

Tumor-bearing mice were killed by cervical dislocation. Fresh tumor tissue (100–200 mg) was washed in ice-cold PBS, transferred to 10 mL of ice-cold DMEM containing 10% FBS, and cut into small pieces. The mixture was centrifuged at 300 × *g* for 5 min at 4°C and the pellet was resuspended in 10 mL of DMEM containing 450 units/mL collagenase IV and 0.1 mg/mL DNase I. After initial digestion for 15 min at 37°C with vigorous shaking, an additional 1 mL of 4,500 units/mL collagenase IV and 1 mL of 1 mg/mL DNase I were added under aseptic conditions, followed by digestion for another 15 min. The solution was centrifuged at 700 × *g* for 10 min at 4°C. The pellets were gently resuspended in 10 mL of ice-cold DMEM with 10% FBS. The cell suspension was filtered through a 70-μm cell strainer, which was rinsed with 10 mL of DMEM containing 10% FBS. The filtered cell suspension was centrifuged at 700 × *g* for 10 min at 4°C and the supernatant was carefully removed. The pellets were gently washed with 10 mL of ice-cold DMEM containing 10% FBS and centrifuged again at 300 × *g* for 5 min at 4°C. The final cell pellets were suspended in 0.3 to 1 mL of immunostaining buffer (PBS containing 2% FBS and 0.1% NaN_3). Cell viability was determined by trypan blue exclusion.

CD31 Immunostaining and Flow Cytometric Analysis

Individual tumors (n = 3–4 per group) were analyzed at each cyclophosphamide treatment time point. First, 2.5×10^5 cells were suspended in 0.1 to 0.2 mL of immunostaining buffer and incubated with 0.25 μg of FITC-conjugated CD31 antibody or isotype control rat immunoglobulin G2a for 60 min at 4°C in the dark. After staining, the cells were washed with ice-cold immunostaining buffer and centrifuged at 300 × *g* for 5 min at 4°C. The pellets were resuspended in 500 μL of immunostaining buffer and analyzed with a FACSCalibur flow cytometer (BD Bioscience) and FlowJo software (Tree Star, Inc.) for data analysis. Total events (100,000–200,000) were counted during fluorescence-activated cell sorting analysis. Both the number of $CD31^+$ cells and the number of total cells were determined. The percentage of $CD31^+$ cells in the total tumor cell population was calculated and the data were expressed as mean ± SE for three to four individual tumors per group.

H&E Staining

Cryosections were fixed in 4% formaldehyde for 15 min at room temperature, washed with PBS, stained in Gill's hematoxylin for 2 min, and then rinsed with tap water. Following 10 dips in 2% acetic acid and then 10 dips in 0.45% NH_4OH, the sections were stained with 1% eosin Y; dehydrated by sequential washings with 95% ethanol, 100% ethanol, and 100% xylene; and then sealed with VectaMount.

TUNEL Assay

The TUNEL assay was done according to the manufacturer's protocol (Promega) with modifications. Tumor cryosections were fixed in 4% paraformaldehyde at room temperature for 15 min. After washing with PBS, the sections were incubated with permeabilization solution containing 1% Triton X-100 (v/v) and 1% sodium citrate (w/v) for 10 min on ice. Following a PBS wash, the sections were fixed again with 4% paraformaldehyde for 5 min. After another PBS wash, the sections were incubated with equilibration buffer for 10 min and then incubated with biotinylated deoxynucleotide triphosphates and terminal deoxynucleotidyl transferase for 1 h at 37°C. Reactions were terminated by washing with 2× SSC buffer (300 mmol/L NaCl, 35 mmol/L sodium citrate) for 15 min. The sections were immersed in 0.3% H_2O_2 for 5 min to block endogenous peroxidase. After incubation with streptavidin horseradish peroxidase (1:500 diluted in PBS) for 30 min, VIP was used as the peroxidase substrate. Color development was terminated by rinsing the slides in tap water. After dehydration, the slides were sealed with VectaMount. The number of TUNEL-positive cells in the entire section was counted at ×200 magnification and the average number of apoptotic cells per field (i.e., apoptotic index) was calculated and expressed as mean ± SE of four individual tumors.

Real-time PCR

TSP-1 and P450 2B11 RNA were quantified in 9L tumors by quantitative real-time PCR using SYBR Green I chemistry. Fresh tissue samples were excised and snap-frozen

in liquid nitrogen, then stored at −80°C. On the days of cyclophosphamide administration, the samples were collected before cyclophosphamide injection. Total RNA was isolated from frozen tissue samples (0.1–0.4 g) using TRIzol reagent according to the manufacturer's protocol. RNA (1 μg) was treated with DNase I for 60 min at 37°C to remove any DNA contamination. After heating for 10 min at 75°C to inactivate the DNase, cDNA was synthesized by reverse transcription in a 20-μL reaction containing random hexamers, MuLV reverse transcriptase, and RNase inhibitor. A 4-μL portion of the final reaction was diluted 1:50 in 50 ng/μL yeast tRNA and used as template DNA for quantitative real-time PCR assays. Forward and reverse quantitative real-time PCR primers were as follows: 18S rRNA, 5′-CGCCGCTAGAGGTGAAATTC-3′ and 5′-CCAGTCGGCATCGTTTATGG-3′; mouse TSP-1, 5′-TGTTCAAGAGGACCGGGCT-3′ and 5′-TGGATGGGTACATCCAGCTCC-3′; rat TSP-1, 5′-CCGGTTTGATCAGAGTGGT-3′ and 5′-GGTTTCGGAAGGTGCAAT-3′; total (rat + mouse) TSP-1, 5′-GGCCAAGATCTATCCAGCCC-3′ and 5′-GCCCACACAGCGTCCAGTA-3′; and P450 2B11, 5′-AAATCCTTCCTCAGGCTCCAA-3′ and 5′-GCCTCCCGTATGGCGTCTAT-3′. Quantitative real-time PCR mixtures containing 8 μL of SYBR Green PCR Master Mix, 4 μL of cDNA, 1 μL of forward or reverse primer, and 2 μL of deionized-distilled water were loaded into triplicate wells of a 384-well plate (5 μL/well) and run through 40 cycles on ABS 7900HT sequence detection system (Applied Biosystems). C_t values determined for each gene were normalized to the 18S rRNA content of the same RNA sample. Data were expressed as mean relative RNA levels for four individual tumors (± SE). The contribution of mouse (host) and rat (9L tumor–derived) TSP-1 RNA to total TSP-1 RNA in solid 9L tumors was determined as follows. 9L rat gliosarcoma tumors grown s.c. do not metastasize and, consequently, host (mouse) TSP-1 accounts for all the TSP-1 RNA detected in mouse liver. By measuring mouse liver TSP-1 RNA levels using both mouse-specific and total (mouse + rat) TSP-1 primer sets, both sets of TSP-1 primer pairs were shown to have similar intrinsic amplification efficiencies (ΔC_t = 12.0 and 12.7, respectively, when normalized relative to 18S rRNA). These two primer sets were used to assay 9L tumor RNA, where the total TSP-1 primer pair detected a substantially higher level of TSP-1 RNA than the mouse-specific TSP-1 primer pair, with rat TSP-1 corresponding to ~95% of the total TSP-1 RNA in untreated 9L tumors after factoring in the <2-fold difference in intrinsic amplification efficiency noted above.

Preparation of Tumor Microsomes and Western Blotting

Frozen tumor samples were homogenized on ice in microsome preparation buffer [100 mmol/L KPi (pH 7.5), 1 mmol/L EDTA, 0.1 mmol/L DTT, 0.1 mmol/L phenylmethylsulfonyl fluoride], centrifuged at 12,000 × *g* for 20 min at 4°C, and the supernatant was collected. The pellet was resuspended in microsome preparation buffer and centrifuged again. The combined supernatants were centrifuged at 185,000 × *g* for 60 min at 4°C. The pellets were washed and resuspended in microsome storage buffer [100 mmol/L KPi (pH 7.5), 1 mmol/L EDTA, 0.1 mmol/L DTT, 0.1 mmol/L phenylmethylsulfonyl fluoride, 20% glycerol]. Protein concentrations were determined with Bio-Rad Dc Protein Assay kit. For Western blot analysis, microsomal protein (20 μg) was electrophoresed on 7.5% SDS-polyacrylamide gels and transferred onto nitrocellulose membranes. Membranes were blocked with 3% fat-free milk in TBST [1 mmol/L Tris-HCl (pH 7.6), 150 mmol/L sodium chloride, 0.1% Tween 20] and probed for 1 h at room temperature with rabbit polyclonal anti–P450 2B11 antibody (1:2,000 in blocking solution). The blot was washed and incubated with horseradish peroxidase–conjugated antirabbit immunoglobulin G (1:3,000 dilution). P450 2B11 protein was visualized with enhanced chemiluminescence detection reagent and exposed to Kodak X-OMAT blue film XB-1. A duplicate gel was stained with Coomassie blue R-250 to confirm equal protein loading for each sample.

Statistical Analysis

Results were expressed as mean ± SE. Statistical significance of differences was assessed by two-tailed Student's *t* test or one-way ANOVA, implemented using Prism software (version 4, GraphPad). $P < 0.05$ was considered statistically significant.

Results

Effect of Intratumoral P450 on Antiangiogenic Action of Metronomic Cyclophosphamide

Metronomic cyclophosphamide treatment substantially regresses 9L tumors, whereas cyclophosphamide treatment on a MTD schedule leads to only a modest delay in tumor growth (13). In the case of 9L tumors that express P450 2B11, a highly efficient catalyst of cyclophosphamide activation, the regression induced by metronomic cyclophosphamide is more rapid and substantially more complete (20). To better understand the mechanism underlying this enhanced antitumor response, we investigated the effect of metronomic cyclophosphamide on tumor vascularization, both in 9L tumors and in 9L tumors expressing P450 2B11 (9L/2B11 tumors). Untreated 9L tumors were highly vascularized, as visualized by CD31 immunostaining (Fig. 1A). The first cycle of metronomic cyclophosphamide treatment had no effect on tumor microvessel density, whereas the second cyclophosphamide treatment induced a notable decrease in microvessel density in both 9L tumors and 9L/2B11 tumors (Fig. 1B). 9L tumor microvessel density continued to decrease slowly after the third cyclophosphamide injection, with no microvessel size selection apparent based on the sizes of the remaining blood vessels. In addition, double immunostaining for CD31 and smooth muscle actin-α revealed a transient increase in the pericyte coverage of tumor blood vessels 3 days after the second cyclophosphamide treatment (Supplementary Fig. S1; day 9, $P < 0.01$),[1]

[1] Supplementary material for this article is available at Molecular Cancer Therapeutics Online (http://mct.aacrjournals.org/).

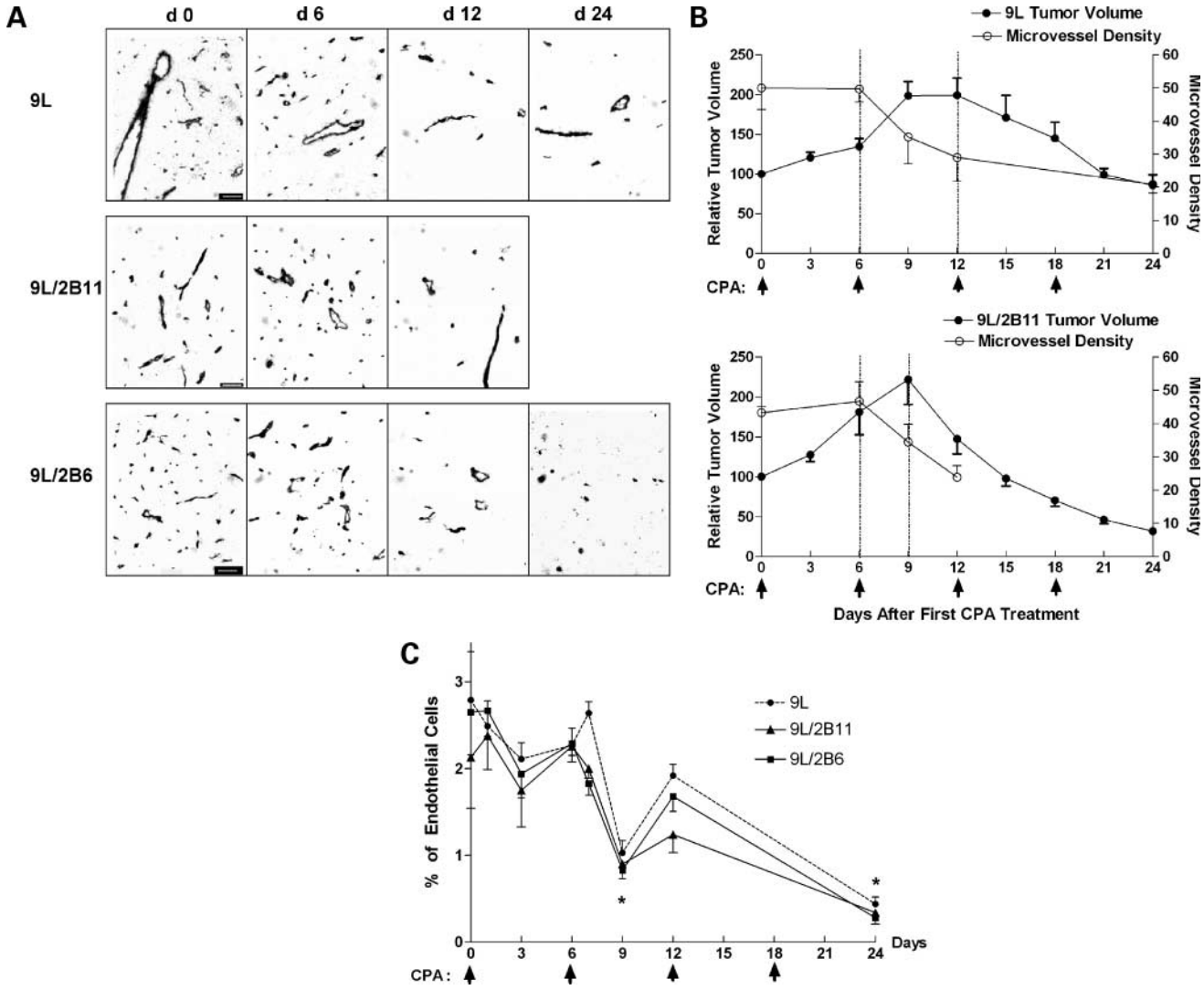

Figure 1. Effect of metronomic cyclophosphamide treatment on growth, vascularity, and endothelial cell population in 9L and 9L/2B tumors. **A,** SCID mice implanted s.c. with 9L control (*top*), 9L/2B11 (*middle*), or 9L/2B6 tumors (*bottom*) were treated with 140 mg cyclophosphamide/kg body weight (i.p. injection) every 6 d beginning when the average tumor volume reached ~500 mm^3. Tumor blood vessels in 9L and 9L/P450 tumor sections were stained with antibody to the endothelial cell marker CD31 on days 0 to 24 after beginning of metronomic cyclophosphamide treatment. Untreated 9L tumors were highly vascularized (day 0). Bar, 50 μm (day 0). **B,** 9L/2B11 tumors began to regress rapidly by day 9, i.e., 3 d after the second cyclophosphamide (*CPA*) injection (*bottom*) whereas 9L tumor regression was slower and began several days later (*top*). A decrease in tumor microvessel density preceded the onset of tumor regression in both 9L and 9L/2B11 tumors, as delineated by the time window between the vertical dotted lines. Microvessel density is presented as the number of blood vessels per field at ×400 magnification. **C,** endothelial cells present in a single-cell suspension prepared from freshly excised 9L, 9L/2B6, or 9L/2B11 tumors were labeled with FITC-conjugated CD31 antibody and quantified as a percentage of total tumor cell population by flow cytometry. Two cycles of metronomic cyclophosphamide induced a 70% loss of tumor-associated endothelial cells, seen on day 9, which further decreased after the third and fourth cyclophosphamide treatments (day 24). *, $P < 0.05$, compared with the most recent cyclophosphamide treatment day (Student's *t* test). Arrows along the *X*-axis indicate days of cyclophosphamide administration (**B** and **C**).

which returned to the basal, untreated level by day 12 and remained at that level through the fourth cyclophosphamide injection.

To confirm these findings using an independent approach, a single-cell suspension was prepared from freshly excised tumor tissue, and endothelial cells were labeled with anti-CD31 antibody and quantified as a percentage of the total tumor cell population by flow cytometry. In untreated tumors, 2.79 ± 0.56% (9L) or 2.13 ± 0.59% (9L/2B11) of the cells were CD31 positive (Fig. 1C). Following the first cyclophosphamide treatment cycle, after a small change on day 1, the percentage of endothelial cells decreased to 2.11 ± 0.19% (9L) or 1.75 ± 0.42% (9L/2B11) on day 3 and partially recovered to near pretreatment levels by day 6. A more substantial reduction in the endothelial cell population was observed 3 days after the second cyclophosphamide injection (Fig. 1C; day 9 versus day 6, $P < 0.01$) and the recovery by day 12 was more

limited. This finding is consistent with observations in Lewis lung cancer xenografts, where endothelial cell apoptosis was maximal by days 1 to 3 after the second cycle of cyclophosphamide treatment (12). A similar endothelial cell response pattern was observed for 9L/2B6 tumors (Fig. 1C; also see Fig. 1A, *bottom*), which express the cyclophosphamide-activating P450 2B6 and are also chemosensitized to cyclophosphamide, albeit less effectively than in the case of P450 2B11. The successive decreases in endothelial cells relative to the overall tumor cell population seen with each round of cyclophosphamide treatment indicate that the damage to the tumor vasculature cannot be fully repaired before the next cyclophosphamide treatment cycle. As such, the damage accumulates, and by day 6 after the fourth cyclophosphamide treatment endothelial cells account for only 0.34% to 0.44% of the total tumor cell population, corresponding to an 85% reduction from the initial level. The same response was seen in all three tumor types (9L, 9L/2B11, and 9L/2B6), indicating that intratumoral expression of a cyclophosphamide-activating P450 enzyme has little effect on the antiangiogenic activity of metronomic cyclophosphamide.

To better understand the role of antiangiogenesis in metronomic cyclophosphamide–induced tumor regression, we compared the changes in tumor size to the changes in vascular density during the course of cyclophosphamide treatment for both 9L and 9L/2B11 tumors (Fig. 1B). Overall tumor cell density was also examined by H&E staining (Fig. 2). The first cyclophosphamide treatment cycle had no discernable effect on tumor growth. As the tumor volume continued to expand, the initial decrease in endothelial cell population seen at day 3 (Fig. 1C) was reversed by day 6, at which time tumor microvessel density and overall tumor cell density were unchanged. Although 9L and 9L/2B11 tumors both continued to grow in volume for the first 3 days after the second cyclophosphamide injection (Fig. 1B), tumor cell density (Fig. 2) and vascularization (Fig. 1C) both decreased substantially during this time period. Tumor regression after the third and fourth cyclophosphamide injections was accompanied by continued decreases in the endothelial cell population and microvessel density. Thus, the second cyclophosphamide cycle triggers serious and irreversible damage to the tumor vasculature, which could be an important factor in the subsequent decrease in tumor cell density. In addition, the antiangiogenic responses to metronomic cyclophosphamide precede the onset of tumor regression for both 9L and 9L/2B11 tumors, which supports the hypothesis that antiangiogenesis contributes to the observed antitumor activity.

Effect of Metronomic Cyclophosphamide on Angiogenesis Inhibitor TSP-1

TSP-1, an endogenous angiogenesis inhibitor, may be expressed in 9L tumor cells, which are of rat origin, and in tumor-associated host stromal cells including endothelial cells, pericytes, and fibroblasts, which are of mouse origin. Species-specific quantitative real-time PCR primers were therefore designed to specifically monitor the expression of tumor cell (rat) and host (mouse) TSP-1 RNA, as well as total (rat + mouse) TSP-1 RNA. Similarly, antibodies to mouse TSP-1 (antibody sc-12312) or rat + mouse TSP-1 (antibody MS-421) were used to monitor TSP-1 protein.

In untreated 9L tumors, ~95% of total TSP-1 RNA is 9L cell derived (rat TSP-1), with the other 5% derived from host stromal cells, as determined by quantitative real-time PCR analysis with liver TSP-1 RNA as a reference control (see Materials and Methods). Total (rat + mouse) tumor-associated TSP-1 RNA varied up to ~2-fold following metronomic cyclophosphamide treatment (Fig. 3C; one-way ANOVA, $P = 0.36$). This reflects the composite profile of 9L cell TSP-1 RNA, which progressively declined in response to metronomic cyclophosphamide (Fig. 3A), and host cell TSP-1 RNA, which increased transiently after the first two cyclophosphamide injections (Fig. 3B). Immunohistochemical staining of tumor sections with anti–total TSP-1 antibody MS-421 (Fig. 3D) revealed a decline after two cycles of cyclophosphamide treatment, in agreement with the decrease in 9L tumor cell TSP-1 RNA. CD31/TSP-1 double immunostaining with host TSP-1-specific antibody revealed a small number of blood vessels with TSP-1

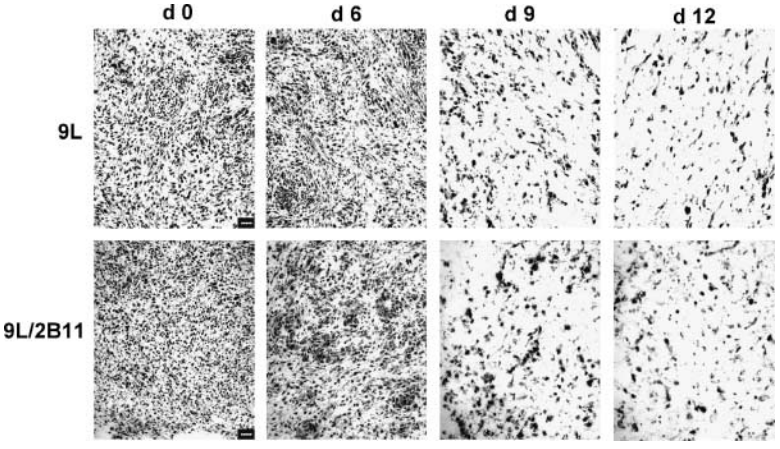

Figure 2. Reduced cell density in 9L and 9L/2B11 tumors treated by metronomic cyclophosphamide. H&E staining revealed a decrease in tumor cell density on the 3rd and 6th days following the second cyclophosphamide treatment (i.e., day 9 and 12). Bar, 50 μm.

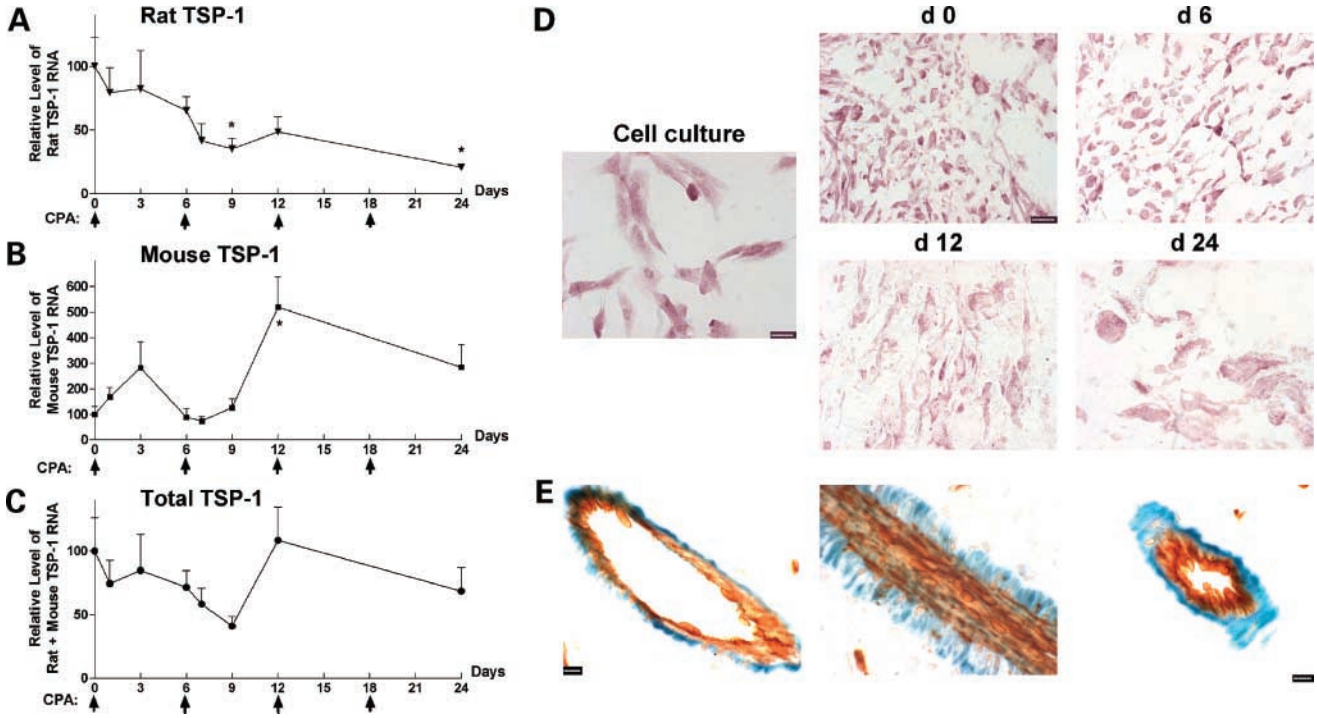

Figure 3. Differential expression of host cell – or tumor cell – derived TSP-1 in metronomic cyclophosphamide – treated 9L tumors. Quantitative real-time PCR analysis of RNA encoding tumor cell – derived rat TSP-1 (**A**), host cell – produced mouse TSP-1 (**B**), and total (rat + mouse) TSP-1 (**C**). *, $P < 0.05$, compared with day 0 (Student's *t* test). Arrows on *X*-axis indicate the days of cyclophosphamide treatment. **D,** antibody MS-421 was used to detect total (rat + mouse) TSP-1 protein in cultured 9L cells and in sections prepared from metronomic cyclophosphamide – treated 9L tumors (days 0 – 24). Bar, 20 μm. **E,** CD31 (*brown*) and TSP-1 (*blue*; antibody sc-12312) double immunostaining revealed mouse TSP-1 staining of perivascular cells but not endothelial cells. Bar, 10 μm.

protein in perivascular cells (Fig. 3E), but not in the associated endothelial cells. Thus, tumor cell and host cell TSP-1 respond differently to metronomic cyclophosphamide, suggesting that each plays a distinct role in the overall antiangiogenic effect.

Intratumoral P450 2B11 Expression Augments 9L Tumor Apoptosis

Next, we investigated why metronomic cyclophosphamide–treated 9L/2B11 tumors regress earlier and more completely than 9L control tumors, given the similar antiangiogenic responses of both tumors. To test whether this difference reflects enhanced killing of the 9L tumor cells by intracellular, P450-dependent activation of cyclophosphamide to 4-OH-cyclophosphamide, tumor cryosections were labeled by TUNEL assay (Fig. 4A) and the apoptotic index was determined for 9L and 9L/2B11 tumors (Fig. 4B). Very few apoptotic cells were detected in untreated tumors. One day after the first cyclophosphamide injection, although there were only small changes in the tumor-associated endothelial cell population (Fig. 1C), the apoptotic index increased significantly in both 9L and 9L/2B11 tumors, indicating a direct antitumor cytotoxic effect of 4-OH-cyclophosphamide. In 9L/2B11, but not 9L tumors, the increase in apoptosis was sustained for 3 days, whereas by day 6, the apoptotic index returned to near basal, pretreatment level in both 9L tumor types (Fig. 4B). During the second cycle of cyclophosphamide treatment, 9L tumors only showed a small, transient increase, whereas in 9L/2B11 tumors, apoptosis increased significantly through the third day, highlighting the P450 2B11–dependent enhancement of tumor cell killing. The enhanced tumor cell cytotoxic response conferred by P450 2B11 is thus distinct from the antiangiogenic action of metronomic cyclophosphamide, which does not differ between 9L and 9L/2B11 tumors.

Response of P450 2B11 Protein to Metronomic Cyclophosphamide

The effect of cyclophosphamide treatment on P450 2B11 RNA and protein was investigated to better understand how intratumoral expression of P450 2B11 contributes to the antitumor effect of metronomic cyclophosphamide. P450 2B11 RNA levels were unchanged in the first two cycles of cyclophosphamide treatment, as determined by quantitative real-time PCR (Fig. 5A). Western blot analysis of microsomal proteins extracted from 9L/2B11 tumors indicated no change in 2B11 protein after the first cyclophosphamide injection. However, by day 12 (i.e., 6 days after the second cyclophosphamide injection), 2B11 protein levels were substantially decreased in all 9L/2B11 tumors (Fig. 5B). Immunohistochemical staining revealed that 29% to 68% of the cells were 2B11 positive in individual untreated 9L/2B11 tumors (average, 55%; $n = 4$

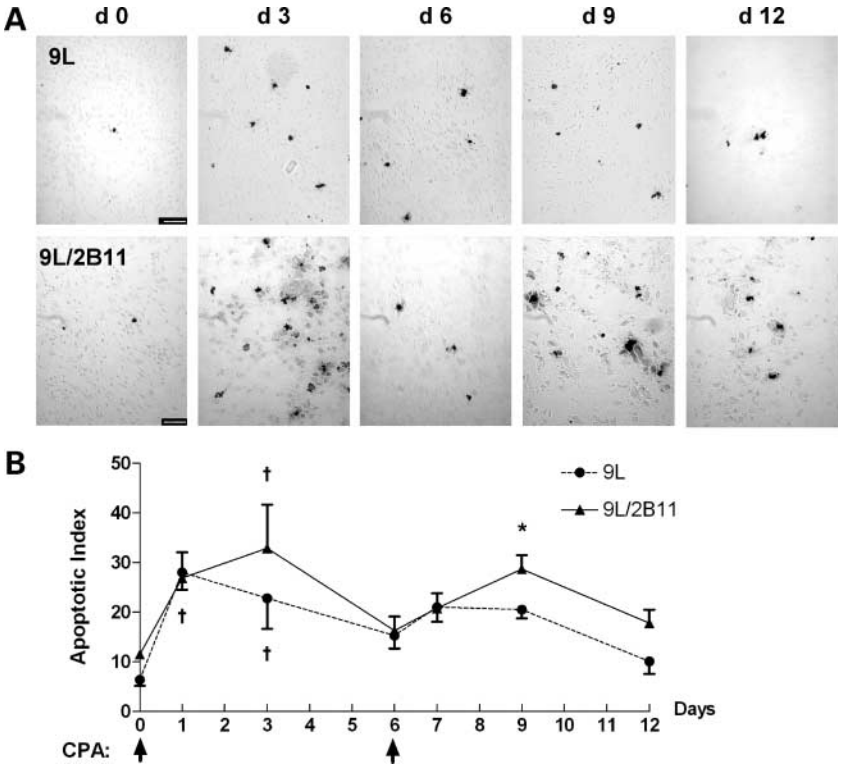

Figure 4. Effect of tumor cell expression of P450 on metronomic cyclophosphamide–induced tumor cell apoptosis. **A,** apoptotic cells in tumor cryosections prepared on days 0 to 12 following initiation of metronomic cyclophosphamide treatment were labeled by TUNEL assay. Very few apoptotic cells were detected in untreated tumors. Bar, 50 μm. **B,** quantification of TUNEL staining in the experiments represented in **A**, as described in Materials and Methods. *, $P < 0.05$, 9L versus 9L/2B11 tumors (Student's *t* test). †, $P < 0.05$, day 0 versus days 1 and 3 (one-way ANOVA, for both 9L and 9L/2B11 tumors).

tumors), as compared with 90% to 95% 2B11-positive cells in the original retrovirus-infected cell population used to implant the 9L/2B11 tumors (Fig. 6A and data not shown). The number of P450 2B11–positive cells was unchanged after the first cyclophosphamide injection but decreased after the second cyclophosphamide treatment (Fig. 6A), consistent with the Western blot results. Similar changes were seen in 9L/2B6 tumors, in which repopulation of the residual tumor mass with P450-deficient cells was apparent by day 24 (Fig. 6A, *bottom*). Many of the remaining P450-positive cells became enlarged and multinucleated in response to metronomic cyclophosphamide, both in the case of 9L/2B11 and 9L/2B6 tumors (Fig. 6B).

Discussion

When cancer chemotherapeutic drugs are administered on a traditional MTD schedule, an obligatory rest period between treatment cycles allows for the recovery of sensitive host tissues (e.g., bone marrow) but also provides an opportunity for recovery and regrowth of tumor cells and tumor-associated endothelial cells. This problem can be circumvented by administration of cyclophosphamide using a regular, repeating (metronomic) schedule, which is associated with antiangiogenic activity (12) and has received much attention as a possible alternative to traditional MTD regimens. When metronomic cyclophosphamide is combined with P450 gene–directed enzyme-prodrug therapy, tumor cell expression of a cyclophosphamide-activating P450 enzyme further enhances activity and leads to a sustained antitumor response (13). Presently, we investigate the effect of intratumoral P450-catalyzed cyclophosphamide activation on tumor-associated endothelial cells and the role of liver versus tumor cell P450 metabolism in the enhanced antitumor response. Our findings lead us to conclude that a close collaboration between hepatic P450 prodrug activation and intratumoral prodrug activation catalyzed by the P450 transgene is required to maximize the therapeutic response in this gene therapy model. Thus, whereas liver P450 prodrug activation alone is sufficient to induce the antiangiogenic effect that is a hallmark of metronomic cyclophosphamide, the small tumors that result retain strong proliferative potential and often become angiogenesis independent. Moreover, the antiangiogenic action of metronomic cyclophosphamide suppresses the uptake of liver-derived 4-OH-cyclophosphamide,[2] thereby rendering the tumor cells resistant to direct cytotoxicity. However, when metronomic cyclophosphamide is combined with intratumoral expression of a cyclophosphamide-activating P450 enzyme, the antiangiogenic effect of liver-activated cyclophosphamide (''killing from the outside'') collaborates with intratumoral P450-dependent cytotoxicity (''killing from the inside'') to enhance overall tumor cell killing, substantially prolonging the tumor-free period after cessation of drug treatment.

An unanticipated finding of the present study was the absence of an effect of intratumoral P450 expression on the

[2] J. Ma and D.J. Waxman, unpublished data.

antiangiogenic action of metronomic cyclophosphamide. Although this finding could be viewed as supporting the hypothesis that the direct antitumor actions of metronomic cyclophosphamide, rather than its antiangiogenic effects, are responsible for the antitumor response seen in the context of P450 gene-directed enzyme-prodrug therapy, that interpretation is not consistent with our earlier finding that regression of 9L/P450 tumors is induced by a metronomic, antiangiogenic cyclophosphamide schedule but not by MTD cyclophosphamide treatment (13). Moreover, various drug-resistant tumor models used in earlier studies confirm the critical role of antiangiogenesis in the antitumor activity of metronomic cyclophosphamide (12). An important feature of P450-based gene-directed enzyme-prodrug therapy using cyclophosphamide is that the active metabolite, 4-OH-cyclophosphamide, readily diffuses across cell membranes and shows a strong bystander cytotoxic effect on surrounding P450-deficient tumor cells, both *in vitro* (22) and *in vivo* (7). However, this bystander cytotoxicity does not extend to include tumor-associated endothelial cells (Fig. 1). This discrepancy could relate to the location of endothelial cells within the tumor. The anatomic structure of the liver determines that hepatocytes have direct access to cyclophosphamide in the blood, enabling liver P450 to dominate cyclophosphamide metabolism following i.p. drug administration. The activated metabolite, 4-OH-cyclophosphamide, enters systemic circulation and reaches the tumor vasculature, where tumor-associated endothelial cells are the first cells to be exposed to 4-OH-cyclophosphamide and its DNA cross-linking, cytotoxic decomposition product phosphoramide mustard. In contrast, 9L tumor cells have more limited access to circulating 4-OH-cyclophosphamide (23), presumably reflecting the dysfunctional tumor vasculature. Moreover, in the case of 9L/2B11 tumors, 4-OH-cyclophosphamide formed intratumorally needs to cross through both tumor stroma and endothelial basal membranes before it can reach tumor-associated endothelial cells. Thus, the extensive exposure of these endothelial cells to liver-derived 4-OH-cyclophosphamide, coupled with their restricted access to 4-OH-cyclophosphamide formed intratumorally, effectively limits the bystander killing of tumor-associated endothelial cells by tumor cell P450-derived 4-OH-cyclophosphamide.

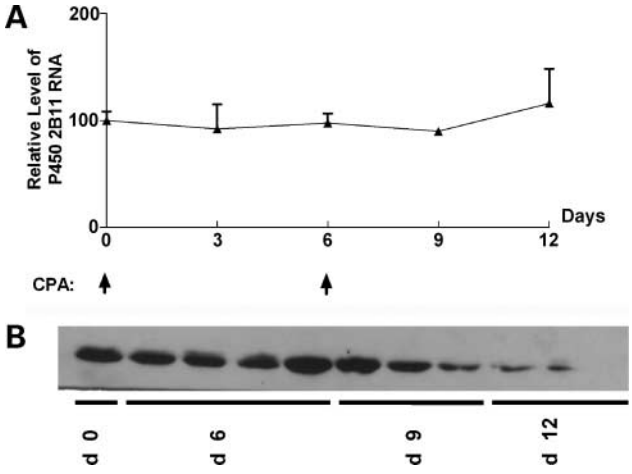

Figure 5. P450 2B11 RNA and protein levels during the course of metronomic cyclophosphamide treatment. **A,** quantitative real-time PCR assay revealed that P450 2B11 RNA levels were unchanged in the first two cycles of cyclophosphamide treatment. **B,** anti–P450 2B11 Western blot of microsomal protein extracts prepared from frozen tumor samples after 0 to 12 days of metronomic cyclophosphamide treatment. Expression of P450 2B11 protein decreased following the second cyclophosphamide injection. By day 12, tumor samples showed little or no detectable P450 2B11 protein (*last three lanes on right*).

In addition to its antiangiogenic activity, metronomic cyclophosphamide shows direct cytotoxicity toward 9L tumor cells, particularly in tumors that express the canine P450 enzyme 2B11, which catalyzes cyclophosphamide activation (4-hydroxylation) with high efficiency due to an atypically low K_m of ~70 μmol/L (20, 21). In 9L tumors, apoptosis induced by the first cyclophosphamide treatment cycle was transient, whereas in 9L/2B11 tumors, tumor cell apoptosis increased substantially until day 3. Moreover, only a limited increase in 9L tumor cell apoptosis was observed following the second cyclophosphamide treatment cycle, suggesting that those tumor cells that are in close proximity to the tumor vasculature and thus are readily accessible to liver-derived 4-OH-cyclophosphamide were already removed in the first cyclophosphamide cycle. Direct killing of the surviving tumor cells may thus occur less frequently in the subsequent cycles of cyclophosphamide treatment. In the case of 9L/2B11 tumors, however, localized prodrug activation was associated with a significant increase in tumor cell apoptosis after the second cyclophosphamide treatment. Three days after the second cyclophosphamide injection, when tumor microvessel density and endothelial cell counts both dropped significantly, antiangiogenesis likely begins to play an important role in the overall antitumor effect. An alternative way to induce strong tumor cell cytotoxicity while retaining the antiangiogenic activity of cyclophosphamide is to combine metronomic treatment with a traditional MTD or bolus schedule (24, 25).

Once activated by P450 enzymes, cyclophosphamide metabolites generated intratumorally kill P450 2B11–positive tumor cells as well as bystander tumor cells. The bystander killing of P450-negative tumor cells is supported by the fact that more complete overall tumor regression is achieved in 9L/2B11 tumors than 9L tumors (20), despite the fact that only 29% to 68% of the tumor cells express P450 2B11 at the time of the initial cyclophosphamide treatment (Fig. 6). Tumor cell P450 2B11 protein, but not RNA, was substantially decreased beginning with the second cyclophosphamide treatment cycle, whereas in the case of another P450 tumor model, 9L/2B6, P450 protein and RNA levels were both unchanged after two cyclophosphamide cycles.[2] This difference may reflect the 20-fold lower K_m (cyclophosphamide) and 28-fold higher V_{max}/K_m ratio exhibited by P450 2B11 compared with P450 2B6 (20), which can result in high intracellular levels of acrolein or other P450 protein-binding metabolites derived from

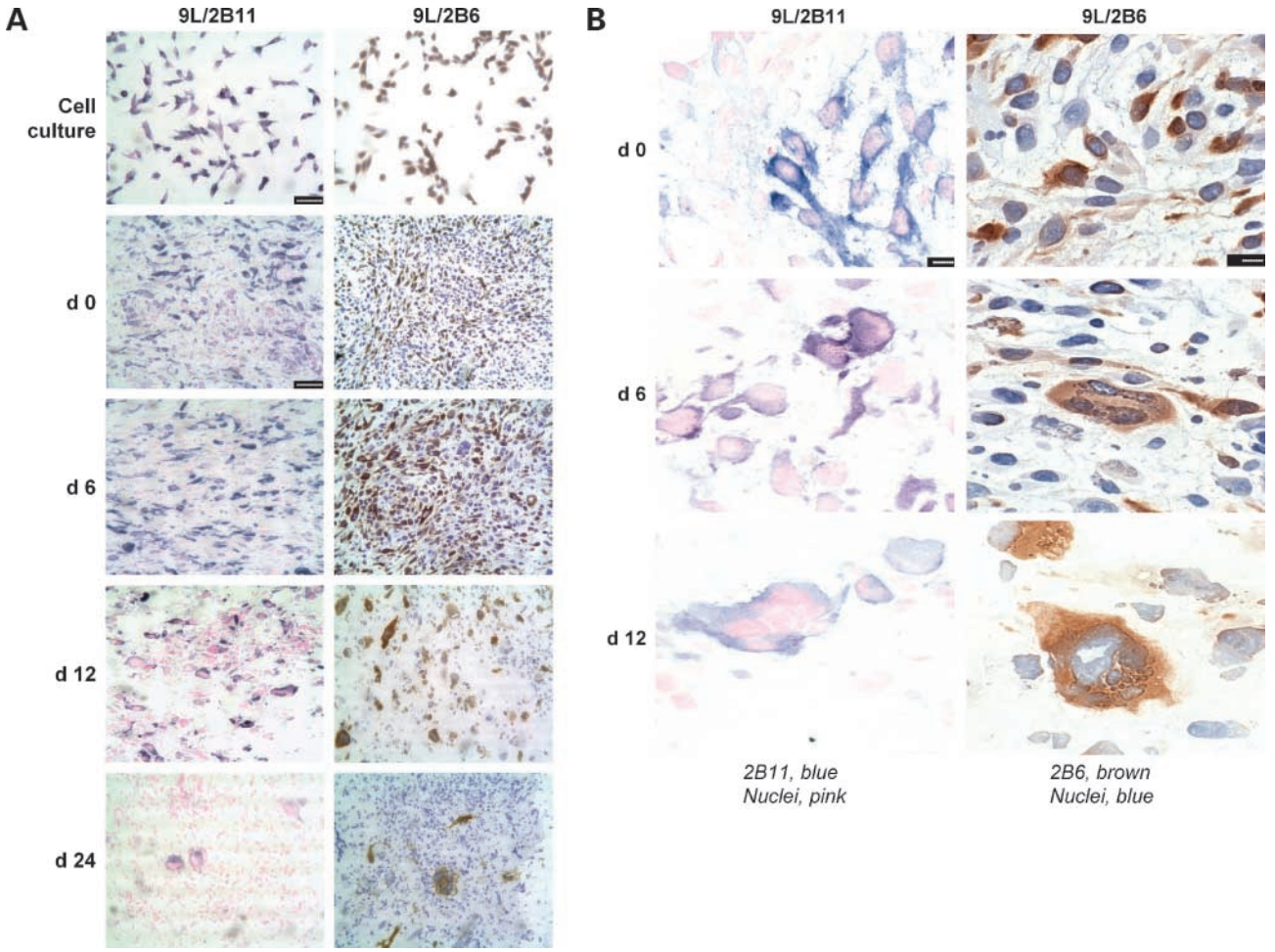

Figure 6. Reduced population of P450-positive cells and their morphologic changes in 9L tumors. **A,** *left,* cultured 9L/2B11 cells (*cell culture*) and 9L/2B11 tumor cryosections (days 0 – 24 after the first metronomic cyclophosphamide injection) were immunostained with anti – P450 2B11 antibody (*blue*) and cell nuclei were labeled by Nuclear Fast Red (*pink*). *Right,* the corresponding set of cultured 9L/2B6 cells and 9L/2B6 tumor cryosections were immunostained with anti – P450 2B6 antibody (*brown*) and cell nuclei were stained with hematoxylin (*blue*). The number of P450-positive cells decreased during metronomic cyclophosphamide treatment, with repopulation by P450-deficient cells evident on day 24, in particular in the case of the 9L/2B6 tumors. Bar, 50 μm. **B,** high-magnification photos show enlarged P450 2B11 – positive (*left*) and P450 2B6 – positive (*right*) cells in sections of cyclophosphamide-treated 9L/2B11 and 9L/2B6 tumors, respectively. These enlarged cells first appeared on day 6. Untreated tumor cells (day 0) are of normal size. Bar, 10 μm.

4-OH-cyclophosphamide (26, 27) and, consequently, P450 protein degradation. The gradual loss of intratumoral P450 protein following metronomic cyclophosphamide treatment indicates that repeated delivery of the therapeutic P450 gene will likely be required to optimize P450-based gene-directed enzyme-prodrug therapy treatment strategies. The death of P450-expressing, 4-OH-cyclophosphamide–producing ''factory'' tumor cells can be delayed, however, by introduction of antiapoptotic factors, which increase the net production of cytotoxic drug metabolites without conferring drug resistance (22, 28).

The decline of P450-expressing tumor cells during the course of metronomic cyclophosphamide treatment was accompanied by a significant enlargement of many of the remaining P450-positive cells, both in the case of 9L/2B11 and 9L/2B6 tumors. Alkylating reagents such as cyclophosphamide induce DNA cross-links, which eventually lead to programmed cell death (29). Cell cycle checkpoints are often perturbed in tumor cells, which can lead to delayed apoptosis and the induction of mitotic catastrophe, as observed in some cytotoxin-treated tumors (30, 31). The enlarged 9L/P450 cells seen in the metronomic cyclophosphamide–treated tumors may thus reflect cyclophosphamide-induced DNA damage culminating in mitotic catastrophe. It is unclear whether the P450 protein that accumulates in these enlarged cells retains cyclophosphamide metabolic activity.

The endogenous angiogenesis inhibitor TSP-1 is expressed in both host tissues (32) and tumor cells (33–36). Its deficiency leads to increased tumor growth and enhanced tumor angiogenesis (37). The antiangiogenic activity of TSP-1 involves multiple mechanisms, including suppression of endothelial cell migration, induction of

apoptosis with increased expression of Fas ligand in proliferating endothelial cells (37, 38), inhibition of vascular endothelial growth factor mobilization in the extracellular matrix, and reduction of blood flow by blocking nitric oxide/cyclic guanosine 3′,5′-monophosphate–induced relaxation of vascular smooth muscle cells (39, 40). The function of 9L cell–derived TSP-1, presently shown to comprise ~95% of the tumor-associated TSP-1 RNA in untreated tumors, is unclear, but it may inhibit the growth of tumor metastases as suggested for other tumors (41–43). Metronomic cyclophosphamide was presently shown to decrease tumor cell (rat) TSP-1 expression while increasing host (mouse) TSP-1, such that a substantial fraction of the 9L tumor–associated TSP-1 is of mouse origin after two cyclophosphamide treatment cycles. CD31/TSP-1 double staining revealed the expression of TSP-1 in host-derived perivascular cells, which is likely an important source of the host TSP-1 detected by quantitative real-time PCR. Metronomic cyclophosphamide induction of TSP-1 has been also observed in perivascular cells associated with Lewis lung cancer and B16F10 melanoma tumors, where either host cell– or tumor cell–derived TSP-1 may augment the antitumor effect of metronomic cyclophosphamide (35). Although the number of TSP-1–positive blood vessels is low in 9L tumors (two to eight vessels per section), the close spatial association between perivascular cells and endothelial cells may facilitate interactions between TSP-1 and its endothelial cell membrane receptor, CD36.

In conclusion, whereas antiangiogenesis clearly contributes to the overall antitumor effect of metronomic cyclophosphamide, the antiangiogenic response is very similar for 9L and 9L/2B11 tumors. It is also apparent, however, that the tumor cell population has poor access to liver-derived 4-OH-cyclophosphamide, especially in the later cycles of metronomic cyclophosphamide treatment, hence the requirement of intratumoral P450 gene delivery and intratumoral prodrug activation for tumor cell elimination leading to a sustained antitumor response. Further increases in intratumoral cyclophosphamide activation could potentially be achieved by direct intratumoral delivery of cyclophosphamide (23) or by inhibition or down-regulation of liver P450 or P450 reductase (44–46), both of which would be expected to increase cyclophosphamide access to tumor-expressed P450 enzymes and enhance intratumoral prodrug activation. Whether the resultant increase in tumor cell–derived 4-OH-cyclophosphamide at the expense of liver-derived 4-OH-cyclophosphamide is consistent with maintenance of the overall antitumor effect requires further investigation.

Acknowledgments

We thank Dr. Youssef Jounaidi of this laboratory for providing the 9L/2B11 and 9L/2B6 cells used in this study, and Chong-Sheng Cheng for assistance in flow cytometry sample preparation.

References

1. Foehr ED, Lorente G, Kuo J, Ram R, Nikolich K, Urfer R. Targeting of the receptor protein tyrosine phosphatase β with a monoclonal antibody delays tumor growth in a glioblastoma model. Cancer Res 2006;66:2271–8.

2. Chu TC, Marks JW III, Lavery LA, et al. Aptamer:toxin conjugates that specifically target prostate tumor cells. Cancer Res 2006;66:5989–92.

3. Kirpotin DB, Drummond DC, Shao Y, et al. Antibody targeting of long-circulating lipidic nanoparticles does not increase tumor localization but does increase internalization in animal models. Cancer Res 2006;66:6732–40.

4. Jounaidi Y, Hecht JE, Waxman DJ. Retroviral transfer of human cytochrome *P*450 genes for oxazaphosphorine-based cancer gene therapy. Cancer Res 1998;58:4391–401.

5. Tyminski E, Leroy S, Terada K, et al. Brain tumor oncolysis with replication-conditional herpes simplex virus type 1 expressing the prodrug-activating genes, CYP2B1 and secreted human intestinal carboxylesterase, in combination with cyclophosphamide and irinotecan. Cancer Res 2005;65:6850–7.

6. Jounaidi Y, Waxman DJ. Use of replication-conditional adenovirus as a helper system to enhance delivery of P450 prodrug-activation genes for cancer therapy. Cancer Res 2004;64:292–303.

7. Samel S, Keese M, Lux A, et al. Peritoneal cancer treatment with CYP2B1 transfected, microencapsulated cells and ifosfamide. Cancer Gene Ther 2006;13:65–73.

8. Salmons B, Lohr M, Gunzburg WH. Treatment of inoperable pancreatic carcinoma using a cell-based local chemotherapy: results of a phase I/II clinical trial. J Gastroenterol 2003;38 Suppl 15:78–84.

9. Braybrooke JP, Slade A, Deplanque G, et al. Phase I study of MetXia-P450 gene therapy and oral cyclophosphamide for patients with advanced breast cancer or melanoma. Clin Cancer Res 2005;11:1512–20.

10. Folkman J. Tumor angiogenesis: therapeutic implications. N Engl J Med 1971;285:1182–6.

11. Jain RK, Duda DG, Clark JW, Loeffler JS. Lessons from phase III clinical trials on anti-VEGF therapy for cancer. Nat Clin Pract Oncol 2006;3:24–40.

12. Browder T, Butterfield CE, Kraling BM, et al. Antiangiogenic scheduling of chemotherapy improves efficacy against experimental drug-resistant cancer. Cancer Res 2000;60:1878–86.

13. Jounaidi Y, Waxman DJ. Frequent, moderate-dose cyclophosphamide administration improves the efficacy of cytochrome *P*-450/cytochrome *P*-450 reductase-based cancer gene therapy. Cancer Res 2001;61:4437–44.

14. Man S, Bocci G, Francia G, et al. Antitumor effects in mice of low-dose (metronomic) cyclophosphamide administered continuously through the drinking water. Cancer Res 2002;62:2731–5.

15. Munoz R, Man S, Shaked Y, et al. Highly efficacious nontoxic preclinical treatment for advanced metastatic breast cancer using combination oral UFT-cyclophosphamide metronomic chemotherapy. Cancer Res 2006;66:3386–91.

16. Klement G, Baruchel S, Rak J, et al. Continuous low-dose therapy with vinblastine and VEGF receptor-2 antibody induces sustained tumor regression without overt toxicity. J Clin Invest 2000;105:R15–24.

17. Colleoni M, Orlando L, Sanna G, et al. Metronomic low-dose oral cyclophosphamide and methotrexate plus or minus thalidomide in metastatic breast cancer: antitumor activity and biological effects. Ann Oncol 2006;17:232–8.

18. Young SD, Whissell M, Noble JC, Cano PO, Lopez PG, Germond CJ. Phase II clinical trial results involving treatment with low-dose daily oral cyclophosphamide, weekly vinblastine, and rofecoxib in patients with advanced solid tumors. Clin Cancer Res 2006;12:3092–8.

19. Bocci G, Tuccori M, Emmenegger U, et al. Cyclophosphamide-methotrexate ''metronomic'' chemotherapy for the palliative treatment of metastatic breast cancer. A comparative pharmacoeconomic evaluation. Ann Oncol 2005;16:1243–52.

20. Jounaidi Y, Chen C-S, Veal GJ, Waxman DJ. Enhanced antitumor activity of P450 prodrug-based gene therapy using the low K_m cyclophosphamide 4-hydroxylase P450 2B11. Mol Cancer Ther 2006;5:541–55.

21. Chen CS, Lin JT, Goss KA, He YA, Halpert JR, Waxman DJ. Activation of the anticancer prodrugs cyclophosphamide and ifosfamide: identification of cytochrome *P*450 2B enzymes and site-specific mutants with improved enzyme kinetics. Mol Pharmacol 2004;65:1278–85.

22. Schwartz PS, Chen CS, Waxman DJ. Enhanced bystander cytotoxicity of P450 gene-directed enzyme prodrug therapy by expression of the antiapoptotic factor p35. Cancer Res 2002;62:6928–37.

23. Chen CS, Jounaidi Y, Su T, Waxman DJ. Enhancement of intratumoral cyclophosphamide pharmacokinetics and anti-tumor activity in a P450 2B11-based cancer gene therapy model. Cancer Gene Ther. Epub 2007 Sep 14 (doi: 10.1038/sj.cgt.7701092).

24. Shaked Y, Emmenegger U, Francia G, et al. Low-dose metronomic combined with intermittent bolus-dose cyclophosphamide is an effective long-term chemotherapy treatment strategy. Cancer Res 2005;65: 7045 – 51.

25. Pietras K, Hanahan D. A multitargeted, metronomic, and maximum-tolerated dose ''chemo-switch'' regimen is antiangiogenic, producing objective responses and survival benefit in a mouse model of cancer. J Clin Oncol 2005;23:939 – 52.

26. Marinello AJ, Bansal SK, Paul B, et al. Metabolism and binding of cyclophosphamide and its metabolite acrolein to rat hepatic microsomal cytochrome *P*-450. Cancer Res 1984;44:4615 – 21.

27. Uchida K, Kanematsu M, Sakai K, et al. Protein-bound acrolein: potential markers for oxidative stress. PNAS 1998;95:4882 – 7.

28. Waxman DJ, Schwartz PS. Harnessing apoptosis for improved anticancer gene therapy. Cancer Res 2003;63:8563 – 72.

29. Schwartz PS, Waxman DJ. Cyclophosphamide induces caspase 9-dependent apoptosis in 9L tumor cells. Mol Pharmacol 2001;60: 1268 – 79.

30. Illidge TM, Cragg MS, Fringes B, Olive P, Erenpreisa JA. Polyploid giant cells provide a survival mechanism for p53 mutant cells after DNA damage. Cell Biol Int 2000;24:621 – 33.

31. Castedo M, Perfettini JL, Roumier T, Andreau K, Medema R, Kroemer G. Cell death by mitotic catastrophe: a molecular definition. Oncogene 2004;23:2825 – 37.

32. Sezaki S, Hirohata S, Iwabu A, et al. Thrombospondin-1 is induced in rat myocardial infarction and its induction is accelerated by ischemia/reperfusion. Exp Biol Med (Maywood) 2005;230:621 – 30.

33. Tringler B, Grimm C, Sliutz G, et al. Immunohistochemical expression of thrombospondin-1 in invasive vulvar squamous cell carcinoma. Gynecol Oncol 2005;99:80 – 3.

34. Naumov GN, Bender E, Zurakowski D, et al. A model of human tumor dormancy: an angiogenic switch from the nonangiogenic phenotype. J Natl Cancer Inst 2006;98:316 – 25.

35. Hamano Y, Sugimoto H, Soubasakos MA, et al. Thrombospondin-1 associated with tumor microenvironment contributes to low-dose cyclophosphamide-mediated endothelial cell apoptosis and tumor growth suppression. Cancer Res 2004;64:1570 – 4.

36. Moon Y, Bottone FG, Jr., McEntee MF, Eling TE. Suppression of tumor cell invasion by cyclooxygenase inhibitors is mediated by thrombospondin-1 via the early growth response gene Egr-1. Mol Cancer Ther 2005;4:1551 – 8.

37. Sund M, Hamano Y, Sugimoto H, et al. Function of endogenous inhibitors of angiogenesis as endothelium-specific tumor suppressors. Proc Natl Acad Sci U S A 2005;102:2934 – 9.

38. Volpert OV, Zaichuk T, Zhou W, et al. Inducer-stimulated Fas targets activated endothelium for destruction by anti-angiogenic thrombospondin-1 and pigment epithelium-derived factor. Nat Med 2002;8:349 – 57.

39. Isenberg JS, Ridnour LA, Perruccio EM, Espey MG, Wink DA, Roberts DD. Thrombospondin-1 inhibits endothelial cell responses to nitric oxide in a cGMP-dependent manner. Proc Natl Acad Sci U S A 2005;102: 13141 – 6.

40. Isenberg JS, Hyodo F, Matsumoto K-I, et al. Thrombospondin-1 limits ischemic tissue survival by inhibiting nitric oxide-mediated vascular smooth muscle relaxation. Blood 2007;109:1945 – 52.

41. Rofstad EK, Graff BA. Thrombospondin-1-mediated metastasis suppression by the primary tumor in human melanoma xenografts. J Invest Dermatol 2001;117:1042 – 9.

42. Crawford SE, Flores-Stadler EM, Huang L, et al. Rapid growth of cutaneous metastases after surgical resection of thrombospondin-secreting small blue round cell tumor of childhood. Hum Pathol 1998;29:1039 – 44.

43. Volpert OV, Lawler J, Bouck NP. A human fibrosarcoma inhibits systemic angiogenesis and the growth of experimental metastases via thrombospondin-1. Proc Natl Acad Sci U S A 1998;95:6343 – 8.

44. Gu J, Chen CS, Wei Y, et al. A mouse model with liver-specific deletion and global suppression of the NADPH-cytochrome *P*450 reductase gene: characterization and utility for *in vivo* studies of cyclophosphamide disposition. J Pharmacol Exp Ther 2007;321:9 – 17.

45. Huang Z, Raychowdhury MK, Waxman DJ. Impact of liver P450 reductase suppression on cyclophosphamide activation, pharmacokinetics and antitumoral activity in a cytochrome *P*450-based cancer gene therapy model. Cancer Gene Ther 2000;7:1034 – 42.

46. Huang Z, Waxman DJ. Modulation of cyclophosphamide-based cytochrome *P*450 gene therapy using liver P450 inhibitors. Cancer Gene Ther 2001;8:450 – 8.